GDL-free multi-phase flow reactors enable stable intermittent CO_2 electrolysis

Max Moran[1], Magda H. Barecka*[1,2]
[1]Department of Chemical Engineering, Northeastern University, 360 Huntington Avenue, Boston, MA, USA
[2]Department of Chemistry and Chemical Biology, Northeastern University, 360 Huntington Avenue, Boston, MA, USA

*corresponding author, m.barecka@northeastern.edu

Contents

Supplementary Notes 3

Supplementary Note 1 3

Supplementary Note 2 6

Supplementary Figures 10

Supplementary Figure 1. 10

Supplementary Figure 2. 11

Supplementary Figure 3. 12

Supplementary Figure 4. 13

Supplementary Figure 5. 14

Supplementary Figure 6. 15

Supplementary Figure 7. 16

Supplementary Figure 8. 17

Supplementary Figure 9. 18

Supplementary Figure 10. 19

Supplementary Figure 11. 20

Supplementary Figure 12. 21

Supplementary Tables 22

Supplementary Table 1. 22

Supplementary Table 2. 23

References 23

Supplementary Notes

Supplementary Note 1

Bubble Tracking and Analysis Pipeline

Analysis code was developed with assistance from Claude (Anthropic, Opus 5). Parameter selection and validation were performed by the authors. Correctness was verified against synthetic data and against manual measurement.

Image Analysis

Detection and Tracking

Videos were recorded at 1080x1920 at 30 fps through the transparent channel plate using a Samsung Galaxy S24. Bubbles were detected in each frame using a Roboflow YOLOv8n object detector trained on 1859 images from 114 videos spanning all current densities and flow rates with various augmentations (flips, rotations, shears, grayscale, hue, saturation, brightness, exposure, blur, and noise) applied to ensure robust detection. Bubbles are tracked between frames using ByteTrack (track activation threshold =0.3, lost-track buffer=30 frames, minimum consecutive frames to confirm a track = 3) in the Roboflow workflow space. Bubble detection produced for every frame a set of bounding boxes with a persistent ID for each bubble (Supplementary Fig. 4).

Calibration

The camera was not in a fixed position between experiments, so a single pixel-length conversion could not be applied across all videos. Calibration was performed independently for each video using the known center to center distance of the reactor screws, which was 20 mm vertically and 12 mm horizontally. Four screw centers were manually placed for the first frame of each video, creating a conversion factor (Supplementary Fig. 6). All positions and lengths reported are expressed in this corrected coordinate system.

To confirm the correct calibration is set for each video and ensure no transposition of the rectangle occurred, the aspect ratio of the selected rectangle is compared to the given dimensions. A disagreement greater than 33% is flagged before calibration is stored. In the dataset of 114 analyzed videos, the stored calibration values is 1.661 ± 0.046 times taller than wide in pixels compared to the 1.67 of the actual values, confirming correct positioning and no transposition. Absolute scale accuracy is assessed in S2.

Velocity

The velocity is calculated utilizing the tracking bounding boxes. The bounding boxes provides three possible points from which to calculate the velocity: leading edge, trailing

edge, and box center. For a bubble that is travelling uninterrupted and unmodified, these would be equal and the center of the box would be used to average any noise from the edges. However, this ideal scenario changes when the bounding box is deforming in the video. This happens when a bubble leaves the channel; the leading-edge stops travelling as the bubble exits the channel and the trailing edge continues to travel shrinking the box. It can also happen when bubbles combine; the leading edge of the first bubble is unaffected, while the trailing edge of the first bubble and the leading edge of the second combine. In both cases, the reported velocity is lower than the true velocity and the bubble center velocity, as the average between the two edges, is also affected.

Supplementary Fig. 7 shows an instance of this where the bubble leading edge is fixed over 48 frames, while the trailing edge traveled 9.8 mm, and the bubble length decreased from 12.4 to 3.1 mm. Using the leading edge would give a velocity of 0.37 mm/s, while the center gives 2.72 mm/s and the trailing edge gives 5.1 mm/s. The other bubbles in this video have a range of 4.6 -7.1 mm/s illustrating the leading edge failure and the trailing edge being the best velocity fit.

As a result, the velocity is determined by analyzing if either edge is pinned to the inlet or outer. This is done by fitting the position against time for the whole trajectory for each of the leading edge, trailing edge, or center. The disagreement between the two edges is defined as D, where D=(difference between edge speeds/larger edge speed). When D ≤0.35, the center was taken as the velocity, and when D>0.35 the slower edge assumed pinned and the faster edge was taken as the velocity. All velocity estimates are reported, along with D for each track so the selection can be examined and revised as needed.

Unit Cell Geometry and Frequency

The unit cell length, L_{UC}, and liquid slug length, L_S, were measured as the center-to-center and edge-to-edge separation of bubbles that were identified in the same frame, and the median was taken over all frames with co-existing bubbles. Gas slug length obtained by difference, L_{UC}-L_S, agrees with the measured bubble length within 2% on average across 103 videos (ratio:0.979 ± 0.124, median 1.007). The two quantities are derived from different routes (bubble-to-bubble spacing versus bounding box height), and provide consistency check on tracking that does not depend on the absolute calibration. The range of values (0.66-1.26) reflects the combined uncertainty of both measurements.

Bubble frequency was determined by diving the bubble velocity over the length of the unit. This is because if the number of bubbles was based on the number counted over the observation window any bubble already in the window as recording starts bias the bubbles per second which can inflate the count.

Validation

Synthetic Validation

Test trajectories with a set velocity, bubble length and spacing were passed through the fitting and selection code used for measurements as a test of the measurement calculations. Velocity, bubble length, unit cell length and liquid slug length were all recovered as the values provided and with 2-pixel positional noise added. The calibration correctly rejected a flipped calibration grid, and a stationary detection was correctly rejected. All checks in the testing pipeline passed.

Manual Validation

Automated measurements were compared with manual frame-by-frame analysis of 19 videos spanning current densities of 2.5-75 mA/cm^2 and flow rates of 1 and 5 cm/s. Bubble velocity was determined by counting the frames required for the leading edge to travel the known screw vertical spacing. Bubble length was measured by selected the leading and trailing bubble edges and was compared against the vertical screw reference. And bubble frequency was measured by counting the number of bubbles passing a location over the video time. The manual validation interface can be seen in Supplementary Fig. 8 and the ratio results can be seen in Supplementary Table 2.

Velocity measurements at 1 cm/s agreed within 5% and had a range of 16% due to the small number of bubbles measured per video. Bubble length is underestimated by approximately 20%. Velocity and bubble length at 5 cm/s are both underestimated by approximately 20% relative to the manual measurement, while frequency agrees within 3%. The deviation here is systematic at this flow rate, so relative comparisons remain valid, but absolute velocities should be treated as lower bounds.

System Limitations

Systematic deviations across all measurements were identified and stated here rather than corrected, so data is reported as measured.

1. Bubble width is overestimated by approximately 16%. The mean measured width is 3.0±0.1 across all videos, while the channel is approximately 2.6mm. This is likely due to additional edge pixels on the bounding box that pad the width measurement. The offset is consistent across the range of videos and conditions.
2. Bubble length is underestimated by approximately 20% relative to the manual measurement. This is likely due to the sensitivity of the detection which can cause the ends of the bubble to be cut off where it is hard to physically see the boundary between the bubble and liquid.

These do not propagate into velocity measurements, since it depends on interface position and sensitivity is consistent throughout the pipeline.

Supplementary Note 2

Utilizing a simple analytical model

Bagemihl et al. developed a simple analytical model that uses electrochemical and transport relations to predict tubular Taylor flow performance [1]. We utilize this model by applying our performance results and calculating the corresponding stagnant thin film thickness. We created a Matlab program to easily analyze our experimental results, which is provided below.

We provided a set of constant values and experimental results to the analytical model. These include electrolyte conditions (dynamic viscosity μ, density ρ, interfacial tension γ, dissolved CO_2 diffusion coefficient D_{CO2}, and saturation concentration of CO_2 c_{CO2}), electrochemical kinetic values (exchange current densities $i_{0,COER}$ $i_{0,HER}$, charge transfer coefficients α_{COER} α_{HER}, and standard electrode potentials E_{CO}^0 E_H^0). The experimental values we provided include the hydraulic diameter of the channel d, the video-extracted flow details (bubble velocity u_B, bubble length L_B, slug length L_S), and electrochemical results $i_{H2,meas}$ $i_{CO,meas}$. Faraday's constant F, gas constant R, ambient temperature T, and pH were provided to the model as well.

We retained all model assumptions about silver kinetics and the stagnant film assumption ($\delta = \delta_F$). The stagnant film assumption is checked after calculation of film thickness.

Our reorganized Bagemihl model begins with calculating an estimated HER overpotential, which is used to calculate the cathode potential and COER overpotential:

$$\eta_{HER} = \frac{RT}{-\alpha_{HER}F}\log\left(\frac{i_{H2,meas}}{i_{0,HER}}\right)$$

$$E_C = \eta_{HER} - 0.059 * pH$$

$$\eta_{COER} = E_C - (E_{0,CO} - 0.059 * pH)$$

We then use the calculated values in a set of Taylor flow equations to determine the film thickness that results in the provided measured partial current density towards CO. This is achieved in Matlab by finding where the provided equation results and the experimental density intersect (Supp Fig. 9). The equations utilized to calculate partial current density are below:

$$Da_{\eta_{COER}} = \frac{i_{0,COER}}{2FC_{CO2}}\exp\left(\frac{-\alpha_{COER}F}{RT}\eta_{COER}\right)\frac{\delta_F}{D_{CO2}}$$

$$\frac{c_{CO2,slugs}}{c_{CO2}} = \left(1 + \frac{L_S + D}{\delta_F}\sqrt{\frac{D_{CO2}\pi}{8du_B}}\frac{Da_{\eta_{COER}}}{1 + Da_{\eta_{COER}}}\right)^{-1}$$

$$k_{ov,CO2} = \frac{D_{CO2}}{\delta_F}\left(\frac{L_B - d}{L_S + L_B} + \frac{L_S + d}{L_S + L_B}\frac{c_{CO2,slugs}}{c_{CO2}}\right)$$

$$i_{CO} = 2Fk_{ov,CO2}c_{CO2}\frac{Da_{\eta_{COER}}}{1 + Da_{\eta_{COER}}}$$

Once the film thickness was determined, we tested the validity of the stagnant film assumption in our case by using the relation:

$$\frac{u_B \delta\delta}{DL_F} < 1$$

The equations above are utilized in Matlab code as shown below:

```
%Values for electrolyte (1M KHCO3)

u = 1001.6*(10^(-6)); %Dynamic viscosity

p = 998.21; %Density

y = 0.07274; %Interfacial Tension

Dco2 = 1.97*(10^(-9)); %Diffusion coefficient of dissolved CO2 in electrolyte


%Values for electrochemical reaction

i0COER = 0.1098; %COER Exchange current density

aCOER = 0.17; %COER charge transfer coefficient

E0CO = -0.11; %Standard electrode potential

i0HER = 4.1439*(10^(-5)); % HER Exchange current density

aHER = 0.25; %HER Charge transfer coefficient

E0H2 = 0; %Standard electrode potential


%Values for Unit Cell Geometry

d = .002; %Hydraulic Diameter of tube in m

uB = .027393; %Bubble velocity in m/s


LB = 0.0145304;%Bubble length
```

```
LS = 0.0043211; %Slug length

CCO2 = 24; %Saturation concentration of CO2
Ca = (u*uB)/y;   %Capillary Number
iH2meas= -333.675; %A/m2;
iCOmeas= -151.695;

%Constants
F = 96485; %Faraday's coefficient
R = 8.3144598; %Universal Gas Constant
T = 298.15; %Ambient Temperature

pH = 8; %pH conditions

nHER = ((R*T)/(-aHER*F))*log(iH2meas/-i0HER)
Ec = nHER -0.059*pH
nCOER = Ec-(E0CO-0.059*pH)
function iCO = f(df, nCOER, i0COER, aCOER, CCO2, Dco2, F, R, T, d, uB, LB, LS)
   Dancoer = (i0COER/(2*F*CCO2))*exp(((-aCOER*F)/(R*T))*nCOER)*(df/Dco2);
   cco2ovcstrco2 = (1+((LS+d)/df)*sqrt((Dco2*pi)/(8*d*uB))*(Dancoer/(1+Dancoer)))^-1;
   kovco2 = (Dco2/df)*(((LB-d)/(LS+LB))+((LS+d)/(LS+LB))*cco2ovcstrco2);
   iCO = 2*F*kovco2*CCO2*(Dancoer/(1+Dancoer));
end
df = fzero(@(x) f(x,nCOER,i0COER,aCOER,CCO2,Dco2,F,R,T,d,uB,LB,LS) -
abs(iCOmeas), [1e-7 1e-3])

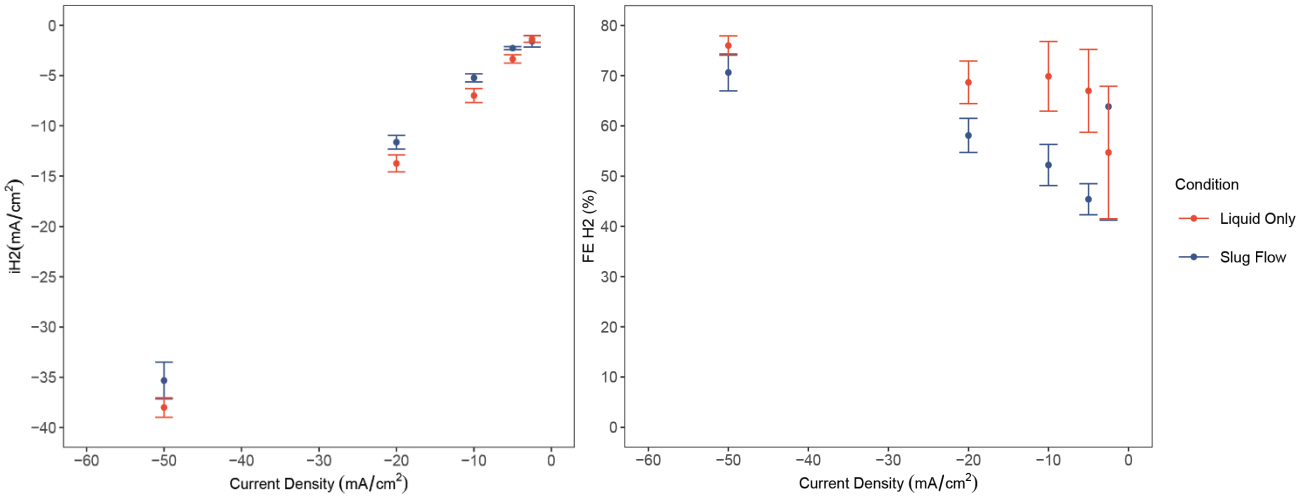
dfs = logspace(-7,-3,300);
```

```
semilogx(dfs*1e6, arrayfun(@(x) f(x,nCOER,i0COER,aCOER,CCO2,Dco2,F,R,T,d,uB,LB,LS), dfs))
yline(abs(iCOmeas))
```

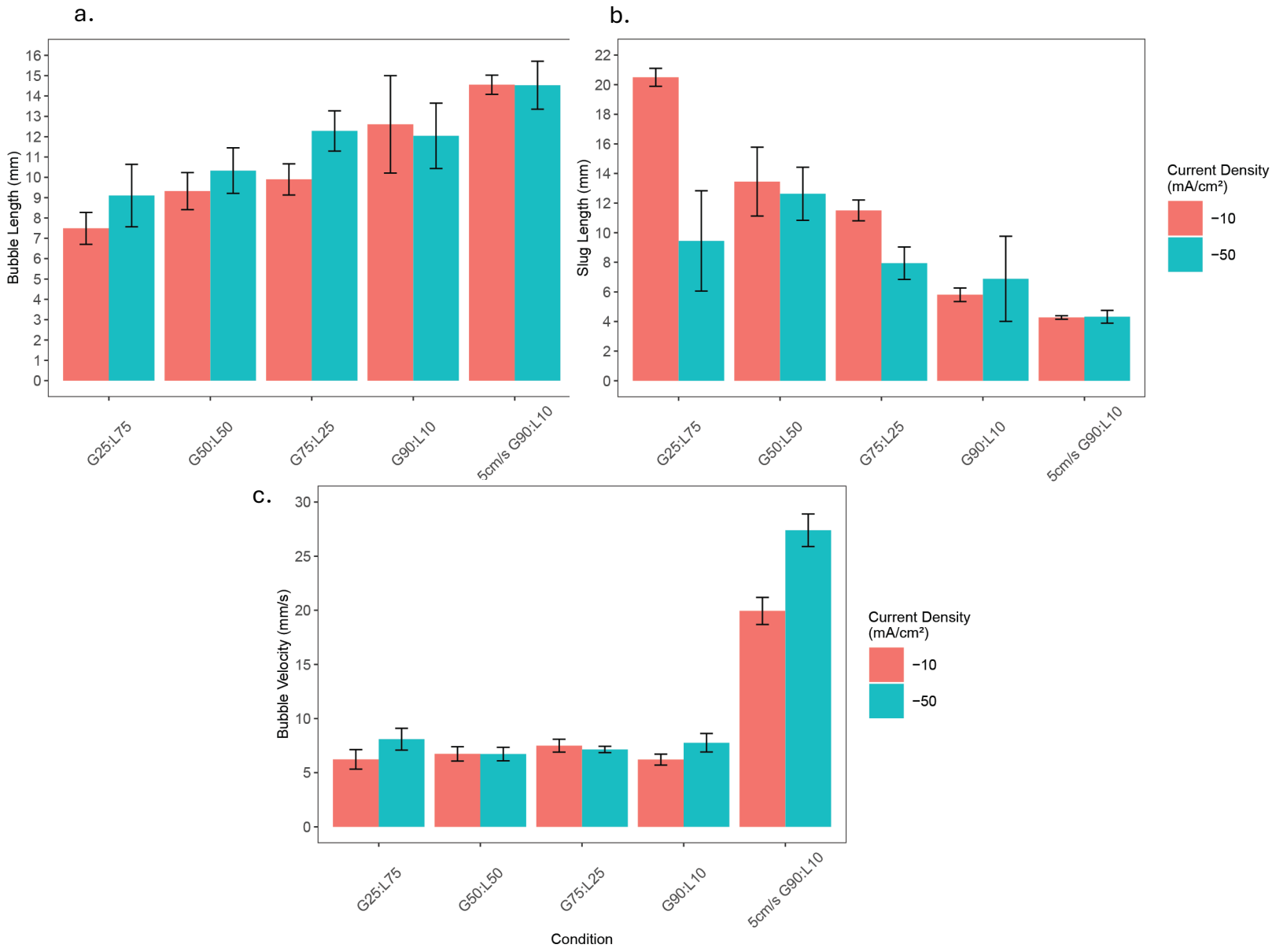
Supplementary Figures

a.

b.

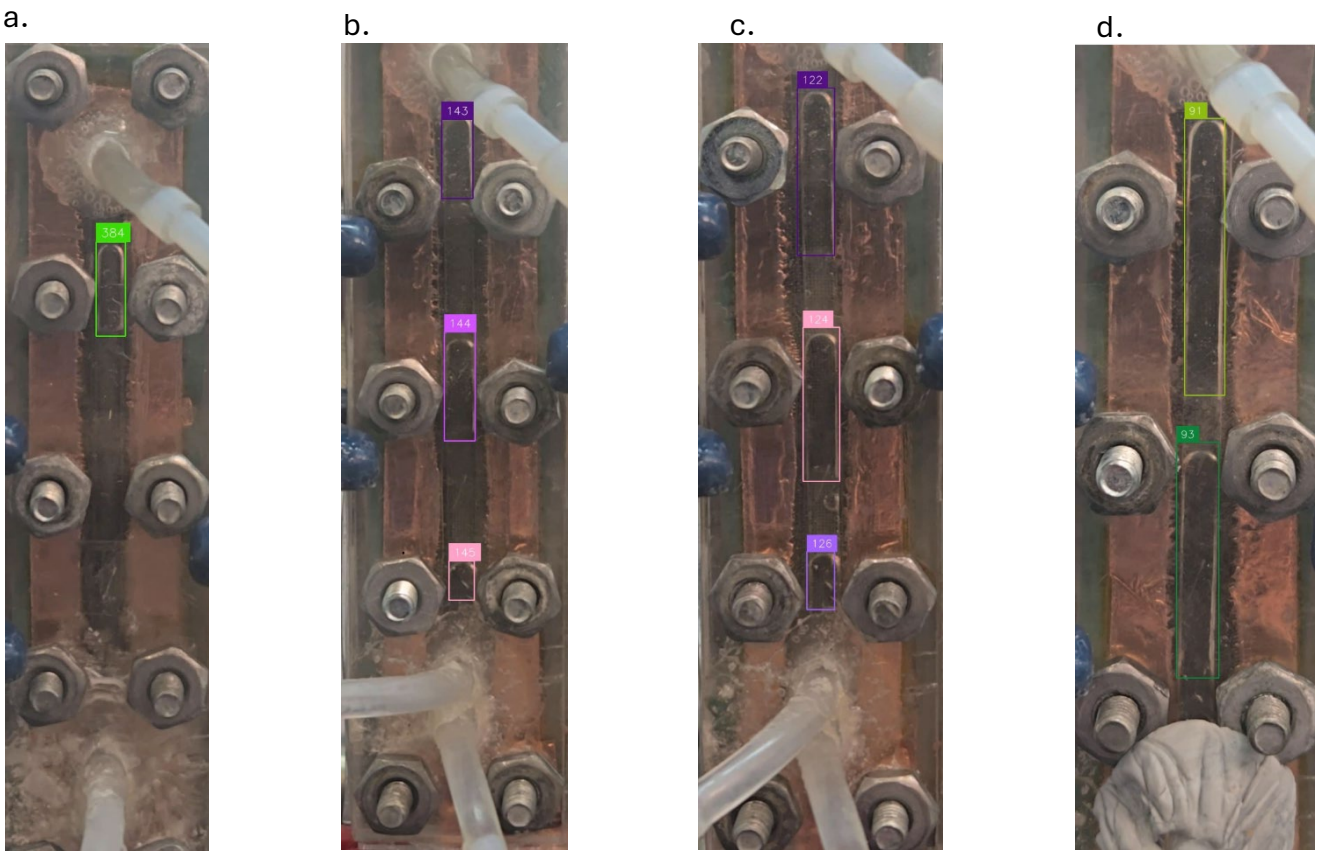


Supplementary Figure 1. Single phase vs multi-phase flow impact on hydrogen evolution reaction (HER). (a) Partial current density towards hydrogen (i_{H2}) over -2.5 to -50 mA/cm^2 for liquid only single-phase flow and slug multi-phase flow. **(b)** Faradaic efficiency towards H_2 over -2.5 to -50 mA/cm^2 for liquid only single-phase flow and slug multi-phase flow.



Supplementary Figure 2.Flow characteristics extracted from video analysis for slug flow at varying gas fractions and total velocity. **(a)** Length of gas bubbles **(b)** Liquid slug length **(c)** Gas bubble velocity.

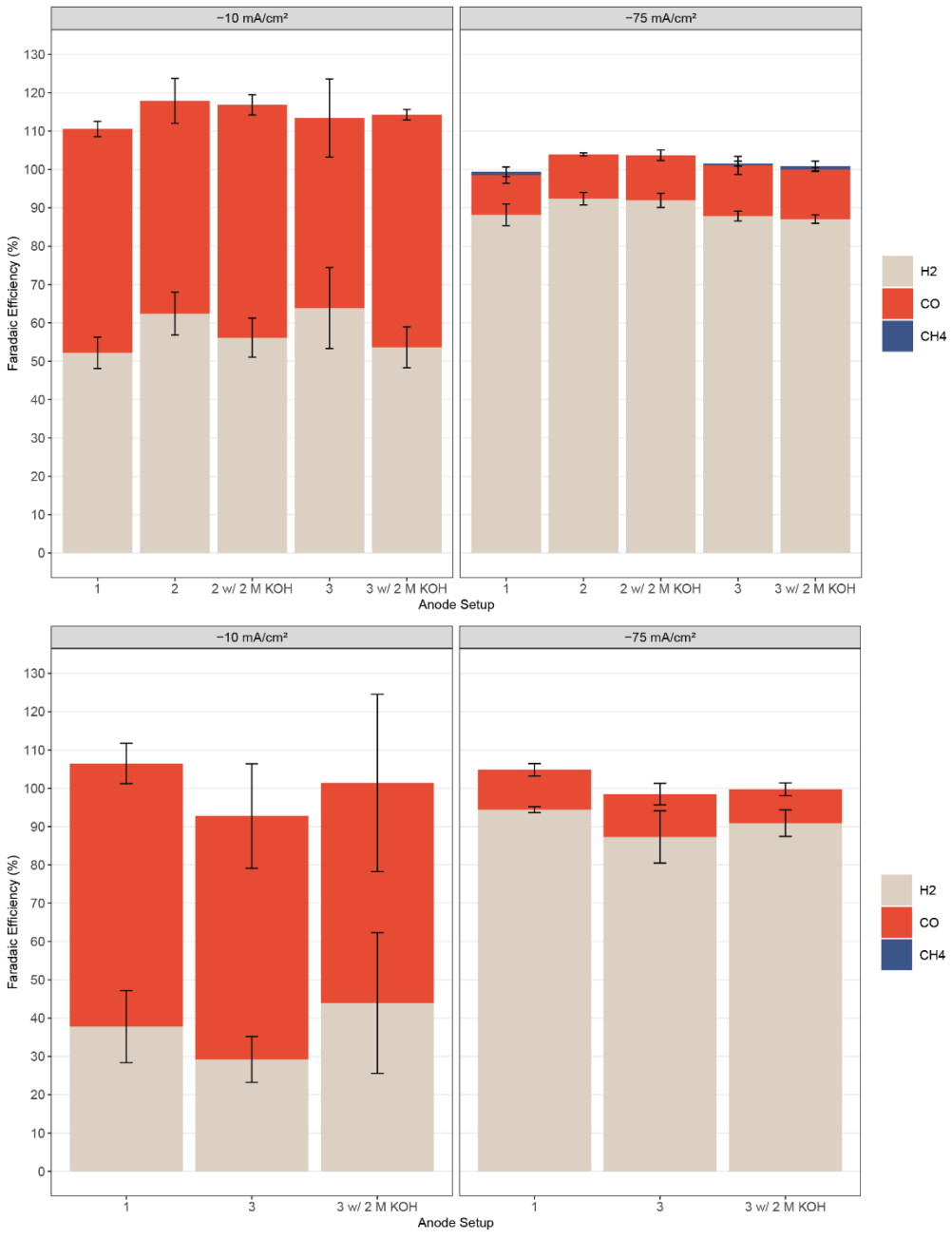
.



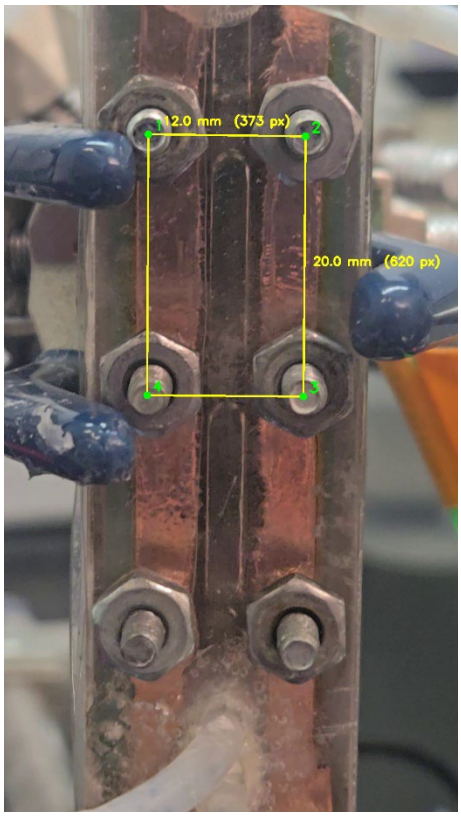
Supplementary Figure 3.Bubble tracking outputs with bounding boxes at various gas fractions. a,0.25 gas, 0.75 liquid. **b,** 0.5 gas, 0.5 liquid. **c,** 0.75 gas, 0.25 liquid. **d,** 0.9 gas, 0.1 liquid.

a.

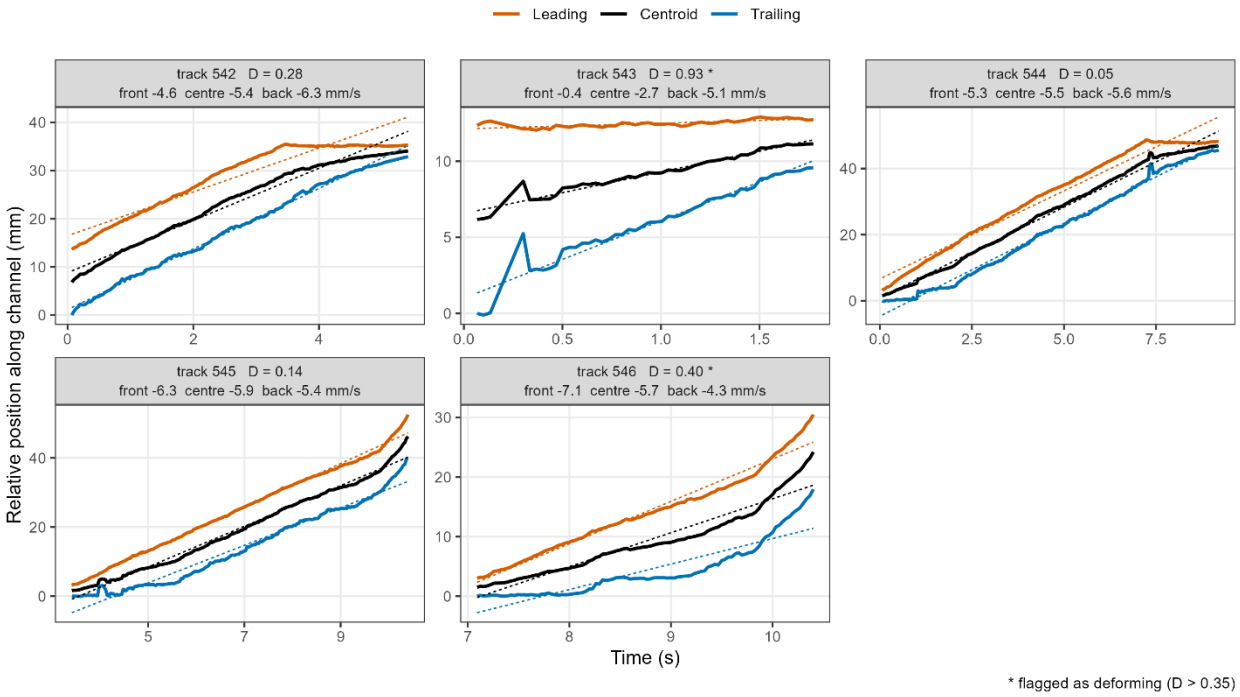
b.



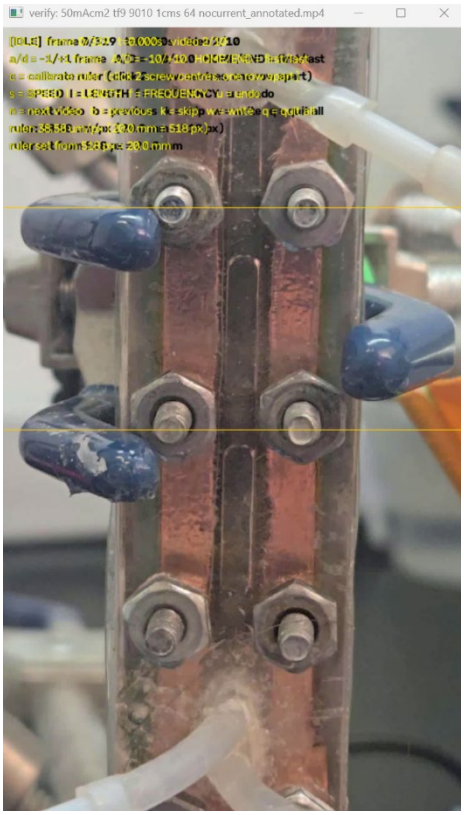
Supplementary Figure 4.Faradaic efficiency comparison between experiment sets with different anode configuration at -10 and -75 mA/cm^2. a, Slug flow configuration. **b,** Annular slug flow configuration.



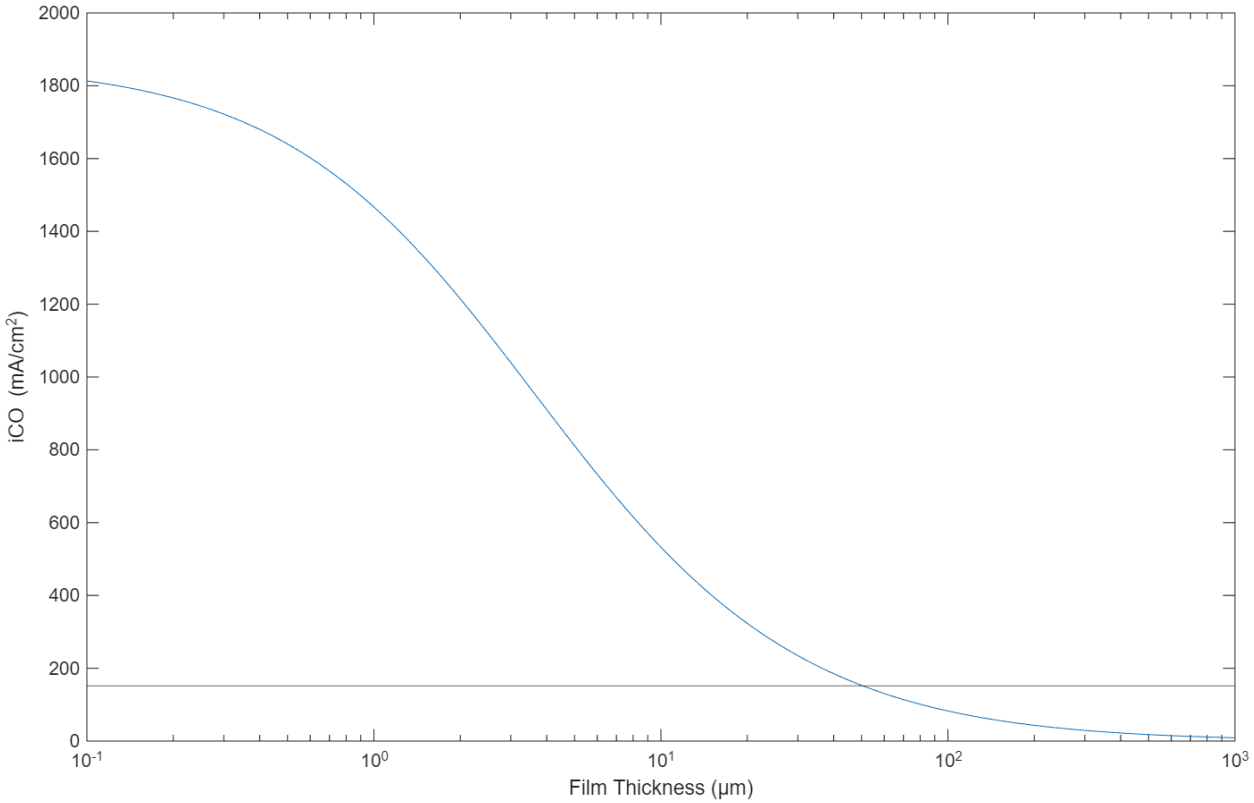
Supplementary Figure 5.Example calibration frame with bolts selected, used to create mm-to-pixel conversion.



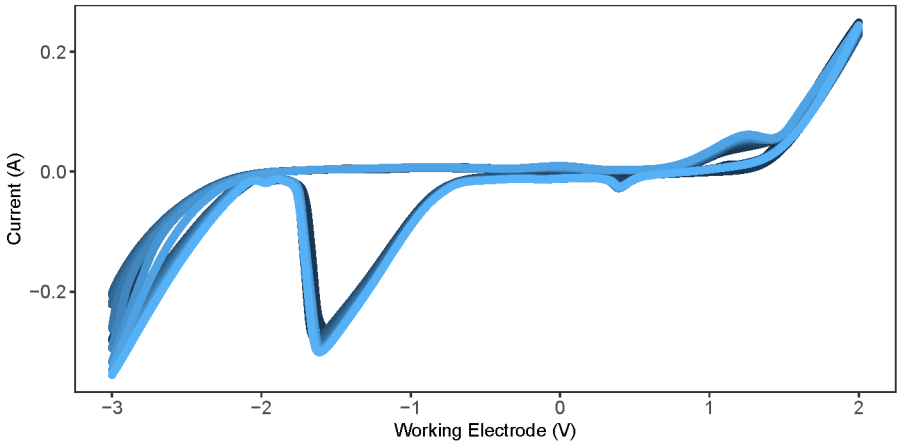
Supplementary Figure 6.Tracks of the leading edge, centroid, and trailing edge of 5 bubbles from a single video. The different bubble parts used for measurement tracked across the video. This illustrates two bubbles that were flagged, track 543 and track 546). Track 543 is an example of when an edge is pinned in a video and does not move affecting the calculations obtained when using the leading edge.



Supplementary Figure 7. Example of a manual validation interface with ruler lines used to track bubble velocity, length and frequency and compare against automated pipeline.

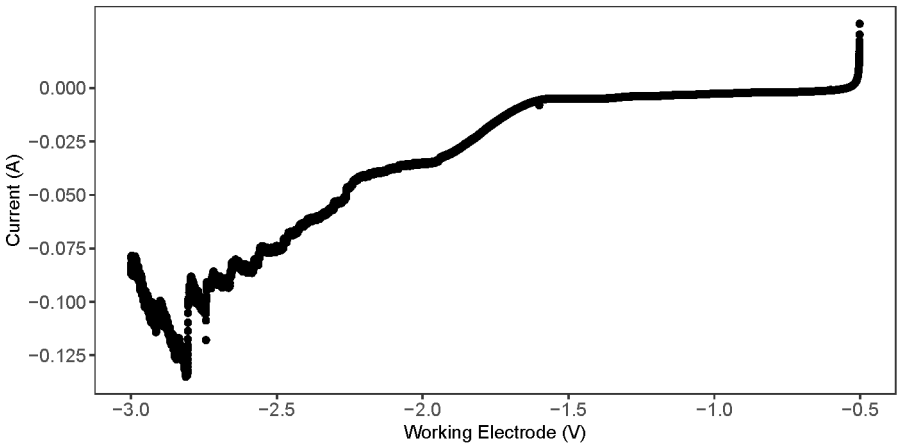


Supplementary Figure 8.Matlab model graphical representation of the calculation of film thickness. The blue line represents the model equations calculated over a range of film thicknesses and the black line is the measured partial current density towards CO from experiments. The intersection is the calculated effective diffusion length.

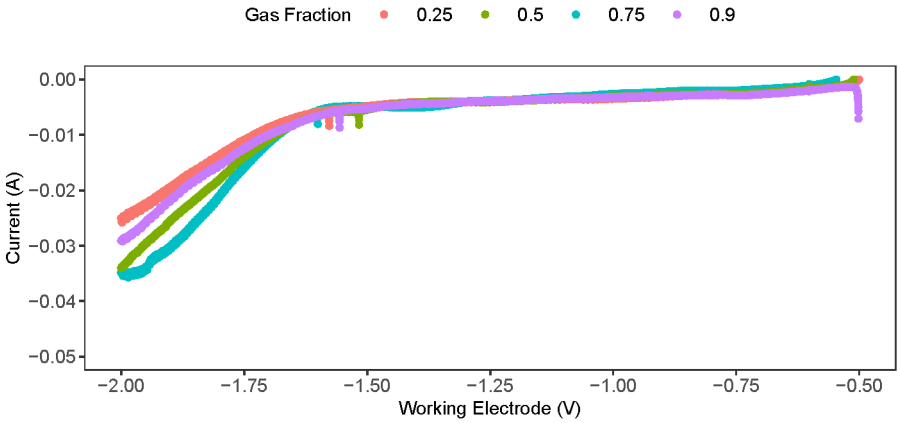


Supplementary Figure 9. Example of cyclic voltammetry pretreatment of silver mesh from +2 to -3V.

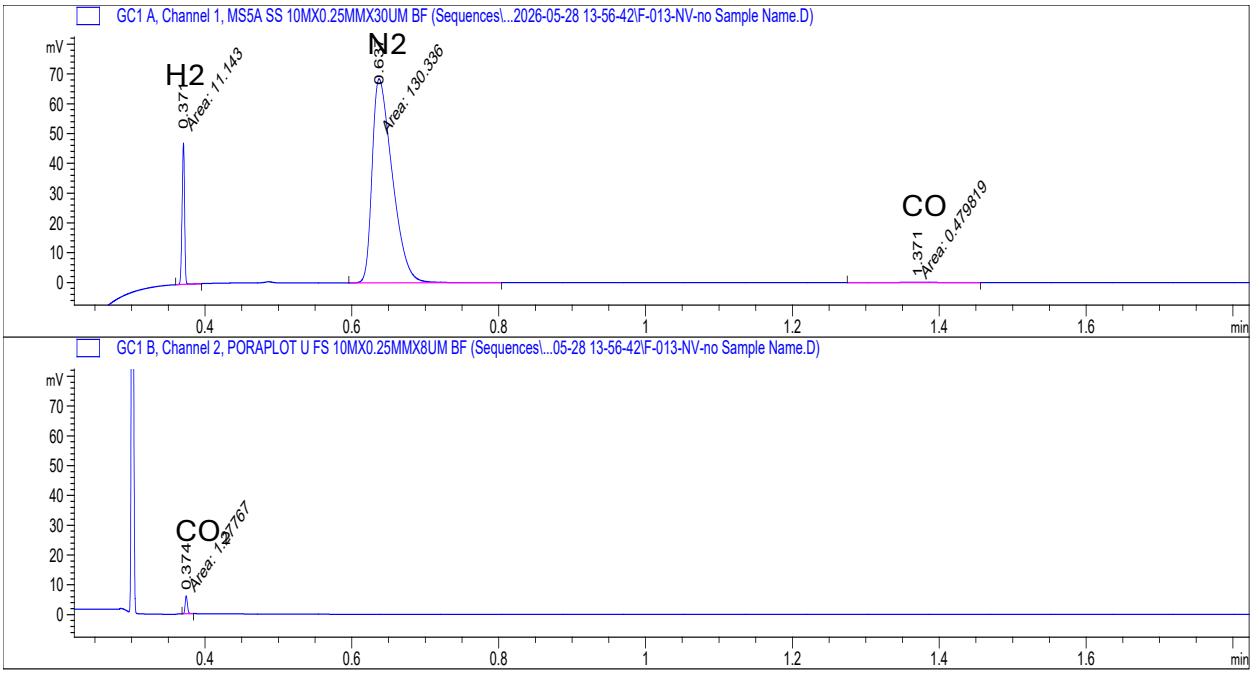
a.



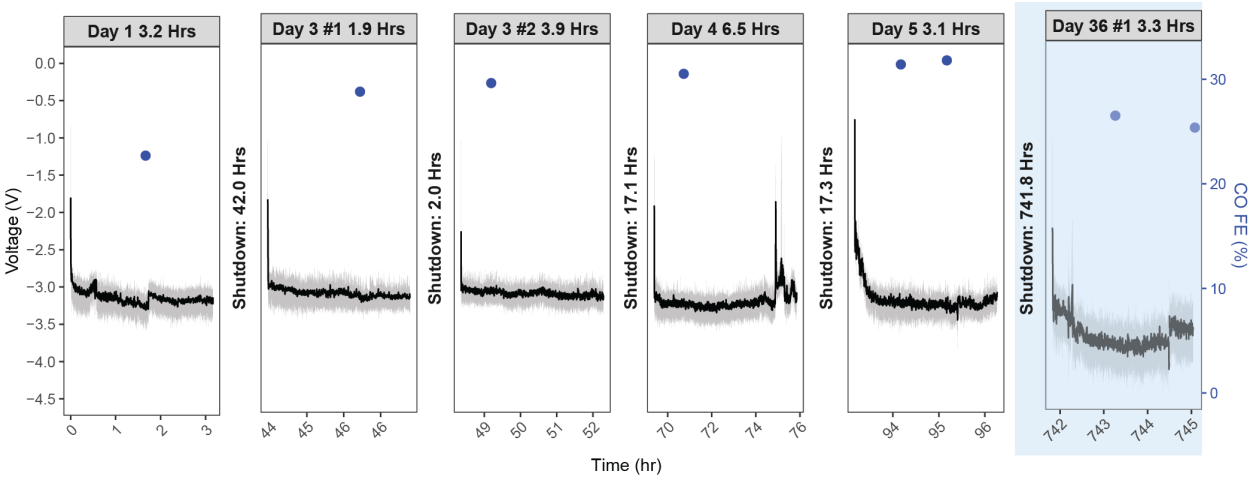
b.



Supplementary Figure 10. Linear sweep voltammetry (LSV) curves performed before CO_2 electrolysis. a, Full LSV curve at 0.75 gas fraction from -0.5 to -3 V. **b,** Zoomed in LSV curve from -0.5 to -2 V at different gas fractions.



Supplementary Figure 11. Example MicroGC 990 output with labeled peaks.



Supplementary Figure 12.Stability test including post-30 day shutdown tests. Dark black line represents voltage average over 10 seconds, gray shaded area represents voltage range fluctuation with sampling interval of 0.1 s, blue shaded boxes represent post-30 day test.

Supplementary Tables

Supplementary Table 1.Flow hydrodynamic with and without applied current. Flow change comparisons for -20 and -50 mA/cm^2 extracted from video analysis.

Output Parameters	-20 mA/cm2		-50 mA/cm^2	
	No Current	Applied Current	No Current	Applied Current
Bubble Velocity mm/s	9.1±0.9	7.6±0.4	8.0±0.6	7.2±0.3
Bubble Length mm	9.4±0.4	10.0±0.6	10.0±0.6	12.3±1.0
Liquid Slug Length mm	15.4±0.5	9.7±0.4	12.9±0.5	7.9±1.1

Supplementary Table 2.Ratio of manually verified measurements to automated pipeline values. Velocity, length, and frequency of bubbles ratios computed during manual validation.

Flow Rate (cm/s)	Velocity	Bubble Length	Frequency
1	1.05±0.16	1.19±0.22	0.93±0.10
5	1.21±0.10	1.22±0.11	1.03±0.07

References

[1] Bagemihl, I., Bhatraju, C., van Ommen, J. R., & van Steijn, V. Electrochemical Reduction of CO_2 in Tubular Flow Cells under Gas–Liquid Taylor Flow. *ACS Sustainable Chemistry & Engineering*, *10*(38), 12580–12587 (2022)